



CFD to VorTECH Pressure-Field Comparison and Roughness Effect on Flow

Sumit Verma¹ and R. Panneer Selvam, F.ASCE²

Abstract: A numerical simulator that very closely resembles the experimental tornado simulator facility called VorTECH at Texas Tech University (TTU) is modeled using three-dimensional simulation. Details of an efficient, simplified computational fluid dynamics (CFD) model without vanes are presented. The pressure field is compared with experimental observations with an emphasis on the vortex breakdown, touchdown, and post-touchdown phase of a tornado. The simulation results indicate that the time-averaged radial ground pressure profile follows a similar trend with the experiment in terms of pressure field distribution. The tornado vortex core is found to be in a transient state in both space and time. The flow at higher swirl ratios has also been observed to lead to greater unsteadiness in flow. Moreover, the effect of roughness on the critical touchdown swirl ratio was also investigated, and increasing roughness length was found to increase the critical touchdown swirl ratio and vice-versa. **DOI: 10.1061/(ASCE)ST.1943-541X.0002766.** © 2020 American Society of Civil Engineers.

Author keywords: 3D simulation; Swirl ratio; Touchdown; Ground pressure; Unsteady flow; Roughness.

Introduction

Different tornado chambers have been in operation in different parts of the world for two decades, of which the major tornado vortex chambers in the world include VorTECH at Texas Tech University (TTU) (Tang et al. 2018), the Iowa State University (ISU) tornado simulator (Haan et al. 2008), and the WindEEE dome at the University of Western Ontario (Hangan 2014). These vortex chambers were built mainly to simulate tornado-like vortices inside a laboratory environment to enable a detailed study to be done on the flow field of the simulated vortices, ultimately serving the end goal of establishing a robust guideline to evaluating the wind loading on built-up infrastructure due to tornadoes. These experimental simulators have been employed to study the flow phenomena, including pressure distribution due to tornadoes, which has provided a valuable fundamental understanding of flow structure and surface pressure distribution due to tornadoes. However, large sums of money are involved to conduct these experimental simulations. Thus, if a well-verified CFD model could be developed, then a detailed study and investigation is possible in a costeffective manner.

In that regard, Liu and Ishihara (2015) compared the time-averaged flow features obtained from their numerical simulator with that of the experimental simulation of Kikitsu et al. (2012) and found that their simulation was a good match, as revealed by the good fit of the data between the experiment and the simulation in terms of ground pressure distribution. However, their simulation was limited to a swirl ratio (S) case of S = 2.44, and the phase of the tornado that is represented by the S value used was

not clearly stated. Because the vortex dynamics and the ground pressure distribution vary significantly due to varying S, a detailed study with varying swirl ratio on the ground pressure distribution is deemed necessary and, thus, forms the central theme of the present work.

Fangping et al. (2016) computed an ISU flow field using their CFD model, but a comparison with the ISU experimental results is lacking. Gairola and Bitsuamlak (2019) modeled the VorTECH simulator, ISU tornado simulator, and WindEEE dome using CFD. However, they did not compare the flow fields with the corresponding experimental simulators. The CFD models were used only to match the experiment for certain configurations. Finally, a simplified model was proposed. Ishihara et al. (2011) proposed a numerical model (based on a Ward-type tornado simulator) with dimensions and configuration similar to that of an experimental simulator used by Matsui and Tamura (2009). However, the comparison was based on a tangential velocity profile, and the study incorporated only two cases of S=0.31 and S=0.65; however, a detailed account on neither touchdown nor the vortex development over the range of swirl ratios was delineated.

Thus, making an exhaustive comparison of the CFD model with experimental observations for touchdown and ground pressure distribution over a range of varying S seems necessary to incorporate all major phases of tornado vortex development. The pressure field is particularly important because the wind load due to straight line (SL) winds is defined in terms of design pressures in the ASCE 7-10 provisions. Several studies (Selvam and Millett 2003) found that the tornadic loads are very different from SL winds; therefore, comprehensively studying wind pressure distribution due to tornadoes seems necessary. In this regard, of particular interest is confining our interest near to the ground surface because most of the structures of our interest, that is, low-rise buildings, fall in that region. To learn more about the near-surface flow field of a tornado, Selvam and Verma (2019) used their simplified three-dimensional (3D) numerical model to investigate and compare the touchdown swirl ratio obtained in their model with that of a TTU experiment and found that their touchdown swirl ratio (S = 0.22) was a good match with the range of S = 0.22-0.36 provided by Tang et al. (2018). In addition to touchdown S, they compared the width of the core radius for different S values and investigated the effect

¹Ph.D. Student, Dept. of Civil Engineering, Univ. of Arkansas, BELL 4190, Fayetteville, AR 72701. ORCID: https://orcid.org/0000-0003-3656-5022. Email: sv015@uark.edu

²Professor, Dept. of Civil Engineering, Univ. of Arkansas, BELL 4190, Fayetteville, AR 72701 (corresponding author). ORCID: https://orcid.org/0000-0003-4944-2718. Email: rps@uark.edu

Note. This manuscript was submitted on June 10, 2019; approved on April 8, 2020; published online on June 29, 2020. Discussion period open until November 29, 2020; separate discussions must be submitted for individual papers. This paper is part of the *Journal of Structural Engineering*, © ASCE, ISSN 0733-9445.

of the variations in the size of the effective hole on the touchdown and core radius.

Selvam and Verma (2019) did not provide an account of ground pressure field variations during touchdown and with varying swirl ratios. Hence, in this work, the ground pressure flow field is compared with the experimental measurements (Tang et al. 2018) and, although attempting to make a pressure field comparison, some interesting phenomena such as the unsteady, time-dependent flow phenomena including vortex wandering were observed in the CFD results. These phenomena are documented in the following sections. In addition, the effect of ground roughness on touchdown is also incorporated in the current study.

The following are the objectives of the current work:

- Demonstrate and provide a detailed account of the unsteady nature of the vortex flow field obtained through the simplified CFD model.
- 2. Investigate the effect of the swirl ratio (S) on the time-dependent nature of the flow in the chamber.
- Develop a method using a Bernoulli equation to relate the inlet pressure to a faraway reference pressure. Because of this approach, the simplified computational domain without inlet vanes can be used for a complicated vortex chamber with an outer box.
- 4. Due to the unsteady nature of the flow, the vortex moves around in time. Hence, comparing the pressure on the ground with VorTECH measurements is a challenge. A method is proposed to compute the pressure for comparison purposes.
- A comparison is made of the radial ground pressure distribution from the CFD model with the experiment.
- Determine the effect of the variation of ground roughness on touchdown.

Numerical Setup

Numerical Simulator Description

The cross-section of the actual TTU vortex chamber and its comparable CFD chamber are provided in Fig. 1. The CFD chamber is modeled as a cylindrical column with an inlet height of h_o and a radius r_o . The aspect ratio (h_o/r_o) of the simulator is kept at unity. The fan outlet in the actual TTU vortex chamber is replaced in the numerical simulator with an effective hole of height 0.4 h_o . A detailed account is available in Selvam and Verma (2019). The Reynolds number for the flow is obtained as 1×10^8 .

Computational Modeling

The 3D incompressible Navier-Stokes (NS) equations in a Cartesian coordinate framework are considered. A large eddy simulation (LES) with a dynamic Smagorinsky model is used for turbulence modeling. The details of the equations are documented in Selvam (1997). In this work, the equations are used in the nondimensional form for efficient computation. The reference values considered for nondimensionalization of the NS equation are (1) inlet height (h_o) for length scale and (2) radial velocity at inlet height (V_{ro}) for the velocity. The reference time $t_{\rm ref}$ is calculated as $t_{ref} = h_o/V_{ro}$. Using these reference values, the nondimensional time (t^*) and pressure (p^*) are obtained from actual time t and pressure p as: $t^* = tV_{ro}/h_o$ and $p^* = p/\rho V_{ro}^2$. The details for the conversion of the dimensional form of NS equations to the nondimensional form can be obtained from Cengel and Cimbala (2014).

Regarding the grid system, first, the semi-staggered grid used in Kashefizadeh et al. (2019) was extended for 3D modeling. This inhouse program provided a checkerboard pressure distribution. Then, for this specific work, a staggered grid was developed in our laboratory. The equations were approximated using a control volume procedure. In the momentum equations, the pressure and diffusion terms are approximated using a central difference scheme. The convection term is approximated using the second-order upwind scheme called Quadratic Upstream Interpolation for Convective Kinematics (QUICK) from Leonard (1979). Further details about the implementation of the scheme can be obtained from Versteeg and Malalasekera (2007). The momentum equation is approximated in time using the Euler backward scheme. The momentum equations are solved by line iteration until the absolute sum of the error for all of the equations reduces to 10^{-5} . The pressure is updated by satisfying the continuity equation using the SOLA procedure reported in Hirt and Cook (1972). The continuity equation error is reduced for each equation below 1×10^{-3} . All of the flow computations and measurements used in the present study were obtained as the result of running the simulation for a total nondimensional time of 25 units.

A grid composition of $75 \times 75 \times 70$ consisting of 393,750 nodes on the basis of an orthogonal grid system is used in the current study to discretize the flow region. Unequal grid spacing is adopted in the x-, y-, and z-directions to optimize the computational time. The aspect ratio of a cell is kept at 5 to obtain much better convergence for the pressure solution, and the circular wall region is introduced by penalizing the outer grid points. The smallest

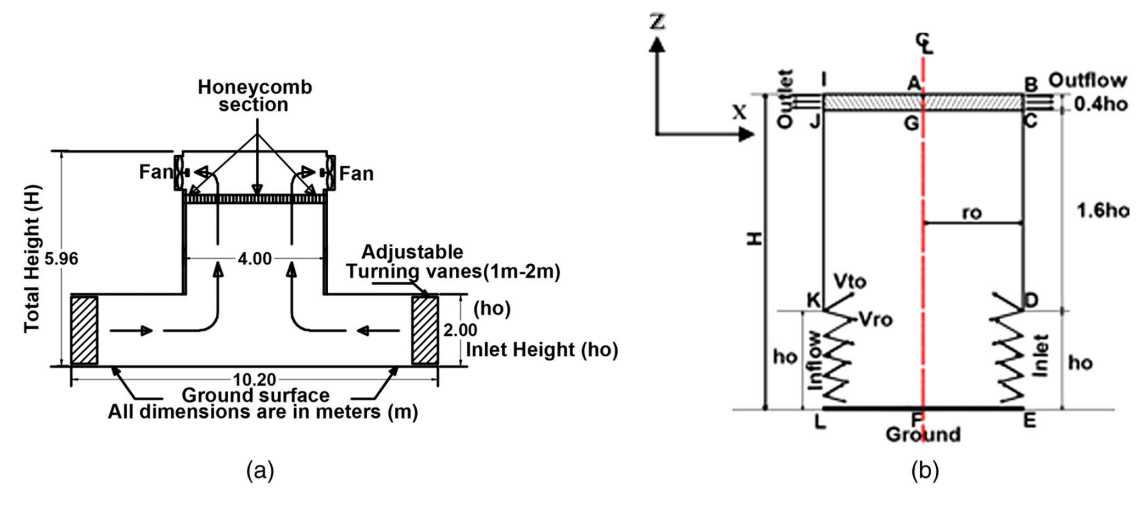


Fig. 1. Cross-section of (a) VorTECH; and (b) corresponding simplified CFD chamber.

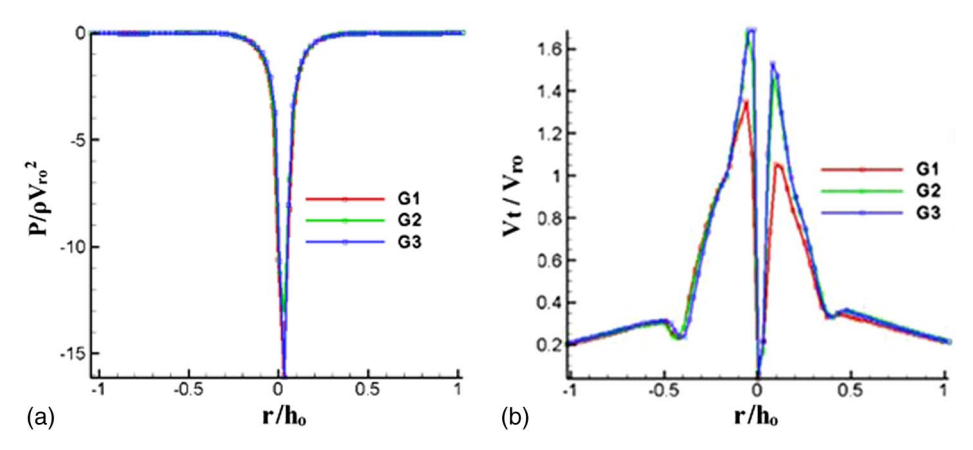


Fig. 2. (a) Radial ground pressure profile for S = 0.15; and (b) tangential velocity profile at elevation (Z) = 0.075 h_a for S = 0.15.

and the largest grid spacing considered are $0.01\ h_o$ and $0.05\ h_o$, respectively. The grid stretching factor for the unequal spacing is kept at 1.1. The grid used in the current study was tested for grid independence, and the mesh details including the obtained results from the mesh are summarized in the section "Grid Independence Test."

Boundary Conditions

The inlet velocities in the x- and y-directions are obtained through a logarithmic velocity profile, and the vertical velocity is considered to be zero. The maximum value of radial velocity component is taken as $V_r(z=1.0) = V_{ro} = 1.0$, and the variation of radial velocity with elevation (z) is given by

$$V_r(z) = C_1 \ln[(z + z_o)/z_o] = C_1 \ln(1 + z/z_o)$$
 (1)

The tangential velocity is obtained from the relation of the swirl ratio $[S=V_{to}/(2V_{ro}h_o/r_o)]$ with the radial velocity component and is given by

$$V_t(z) = 2V_r(z)Sh_o/r_o (2)$$

A uniform normal velocity is provided at the outlet and equals the total inlet velocity. Other velocity components are calculated considering their normal derivatives to be zero. No-slip BC is implemented in the side, bottom, and top walls. The law of the wall is implemented on the walls. Similarly, the roughness parameters used in the model are $z_o = 0.00004 \, h_o$ and $C_1 = 0.0924 \, V_{ro}$.

Grid Independence Test

Three different mesh were considered for grid independence, the details of which are reported in Table 1. The radial ground pressure and the tangential velocity profile were compared from three grids (G1, G2, and G3) at S=0.15 at S=0.15 as shown in Fig. 2. The pressure and tangential velocity profiles were both taken along the diametric axis of the vortex chamber. The pressure profile was taken on the ground plane with the pressure values calculated relative to the inlet of the vortex chamber, whereas the tangential velocity profile was taken at an elevation of $z=0.075\,h_o$ above the ground plane.

The radial ground pressure profile from the grids (G2 and G3) collapses well with the normalized root mean square error (NRMSE) of approximately 3.97%. Similarly, the NRMSE for a tangential velocity profile was obtained at 2%. Because the

Table 1. Different grids for grid independence test with their node count and mesh size

G1	G2	G3
61	75	85
61	75	85
50	70	85
186,050	393,750	614,125
$0.006 h_o$	$0.005 h_o$	$0.004 h_o$
$0.030 h_o$	$0.025 h_o$	$0.020 h_o$
	61 61 50 186,050 0.006 h _o	$\begin{array}{cccc} 61 & 75 \\ 61 & 75 \\ 50 & 70 \\ 186,050 & 393,750 \\ 0.006 h_o & 0.005 h_o \end{array}$

NRMSE values for the radial ground pressure profile and tangential velocity profile are less than 5%, the obtained solution from the grid (G2) was considered to be grid-independent. For further studies and analyses, the grid (G2) will be used unless otherwise stated. To be noted is that the range of the dataset was considered for normalization when calculating the NRMSE for both the ground pressure and the tangential velocity profile.

Similarly, a comparison with the contemporary work of Gairola and Bitsuamlak (2019) reveals that the finest grid resolved 15 cm with a total of 2.9 million grid points, whereas in the current work, the finest grid resolves 2 cm of the actual tornado chamber with the total grid points of 393,750 nodes. Thus, a refined study could be done with the choice of a simplified computational domain without vanes and an outer box.

Results and Interpretation

Unsteady Nature of TTU Vortex Chamber Flow

Because the flow properties such as the velocity and pressure of the fluid were found to change with respect to time, the flow can be said to be unsteady. From CFD visualizations, the vortex core is found to be in a state of transition in both space and time. The temporally transient behavior of the vortex core can be observed in Figs. 3(a and b), in which the pressure isobaric surface of the tornado vortex core exits the tornado vortex chamber through different faces and different angles when the simulation is run for different nondimensional time units. Spatially transient behavior is reported in the section "Phenomena of vortex wandering." As observed in Fig. 3(c), the localized regions with recirculating velocity vectors (represented by red circles) observed in the *yz*-projection plane of the tornado vortex are the twisting regions of the pressure iso-surface.

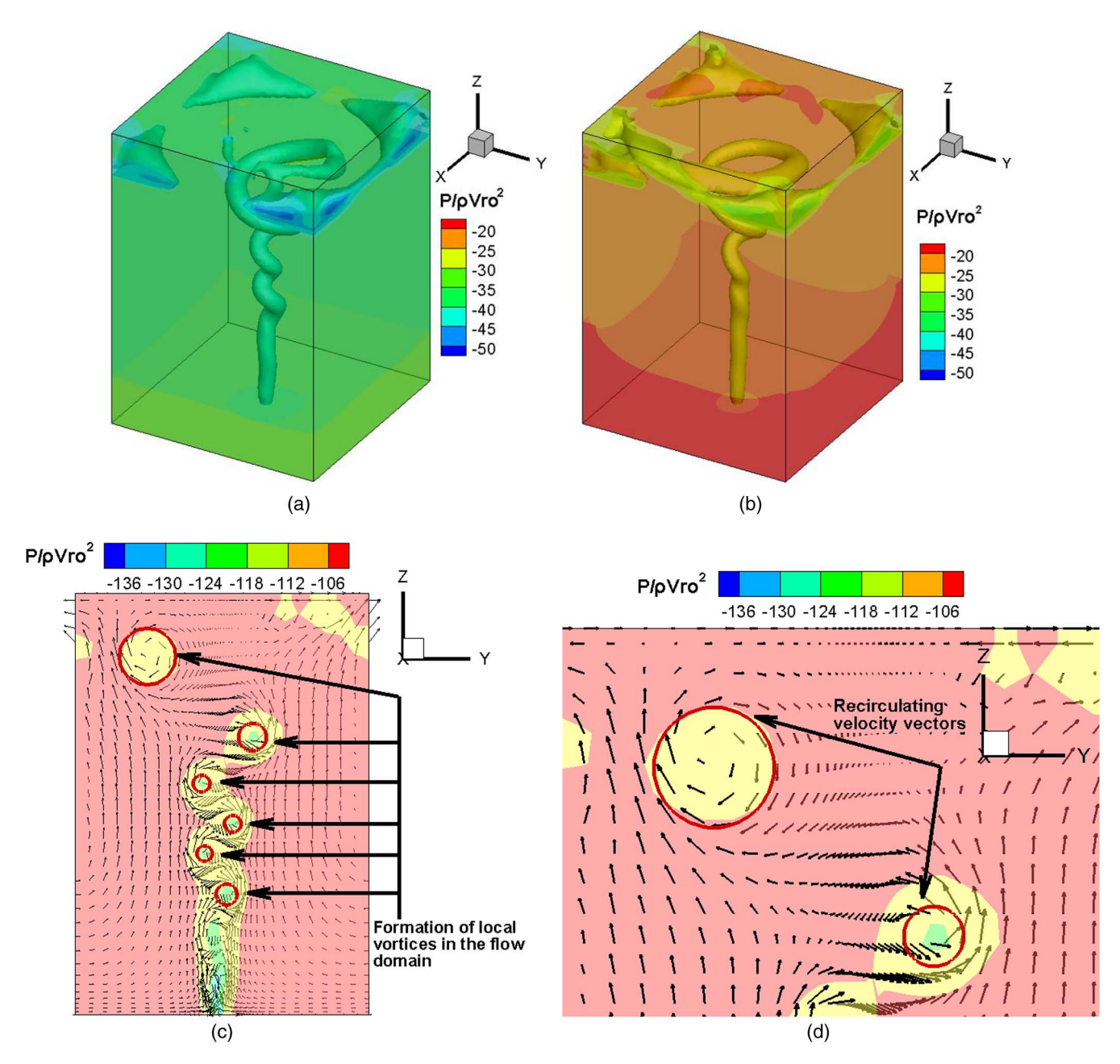


Fig. 3. Nondimensional pressure isosurface for two different times to illustrate unsteady nature of the vortex at S = 0.25: (a) time = 10 units; (b) time = 20 units; (c) twisting region of pressure isosurface in the yz-plane; and (d) zoom-in for (c) recirculating velocity vectors.

For time-varying flow fields, common practice is to average the flow properties over a suitable finite length of time to obtain the mean flow fields to represent the flow characteristics and comparison. Accordingly, special emphasis is placed on the time-dependent flow phenomena observed inside the tornado chamber and is explained in the section "Time-Dependent Flow Phenomena."

Time-Dependent Flow Phenomena

Flow inside the tornado vortex chamber is unsteady and time-dependent, as explained by the time-series data of tangential velocity and pressure (Fig. 4) with an approximate sinusoid waveform-like variation. Given this transient flow behavior, some challenges were encountered to determine the radial ground pressure distribution due to tornado, and the details are included in the sections "Time Averaging Procedure" and "Touchdown S and Effect of

Varying S on Radial Ground Pressure Distribution." The nature of the variation in the waveform of the flow field is an important clue to what length of time should be considered to time-average the flow field parameters to ensure that the averaging procedure is able to properly capture the mean flow field. Thus, an attempt was made to study the effect of unsteadiness in flow on the ground pressure field and the tangential velocity field. When the tangential velocity and ground pressure were tracked at the geometric center of a computational domain with respect to time at S=0.22, it was found to be varying in a cyclic manner, as shown in Fig. 4.

Because the swirl ratio is an essential nondimensional parameter that influences the flow features and the overall dynamics of a tornado and, in this study, a wide range of *S* values were to be considered to analyze the overall development of tornado vortex from the pretouchdown to the posttouchdown phase, the effect of varying *S* on the unsteadiness of flow was studied next. As indicated in

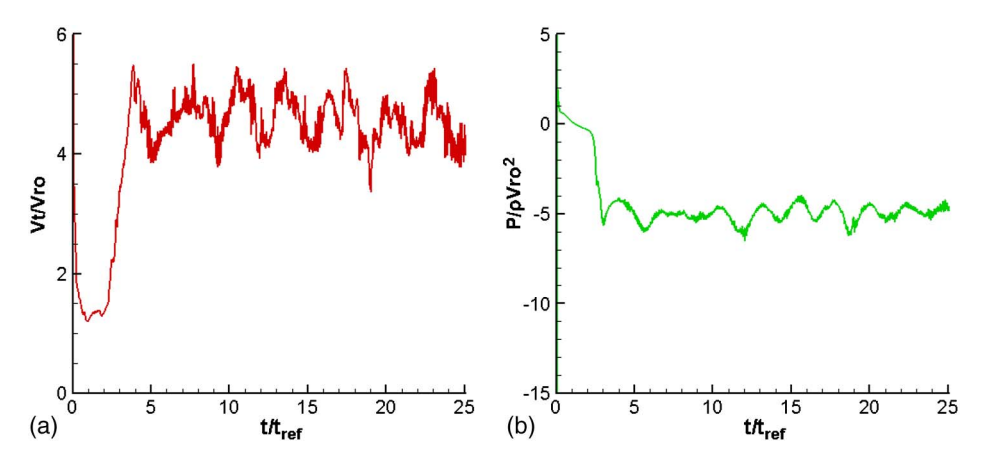


Fig. 4. Variation in (a) tangential velocity; and (b) pressure at geometric center of computational domain.

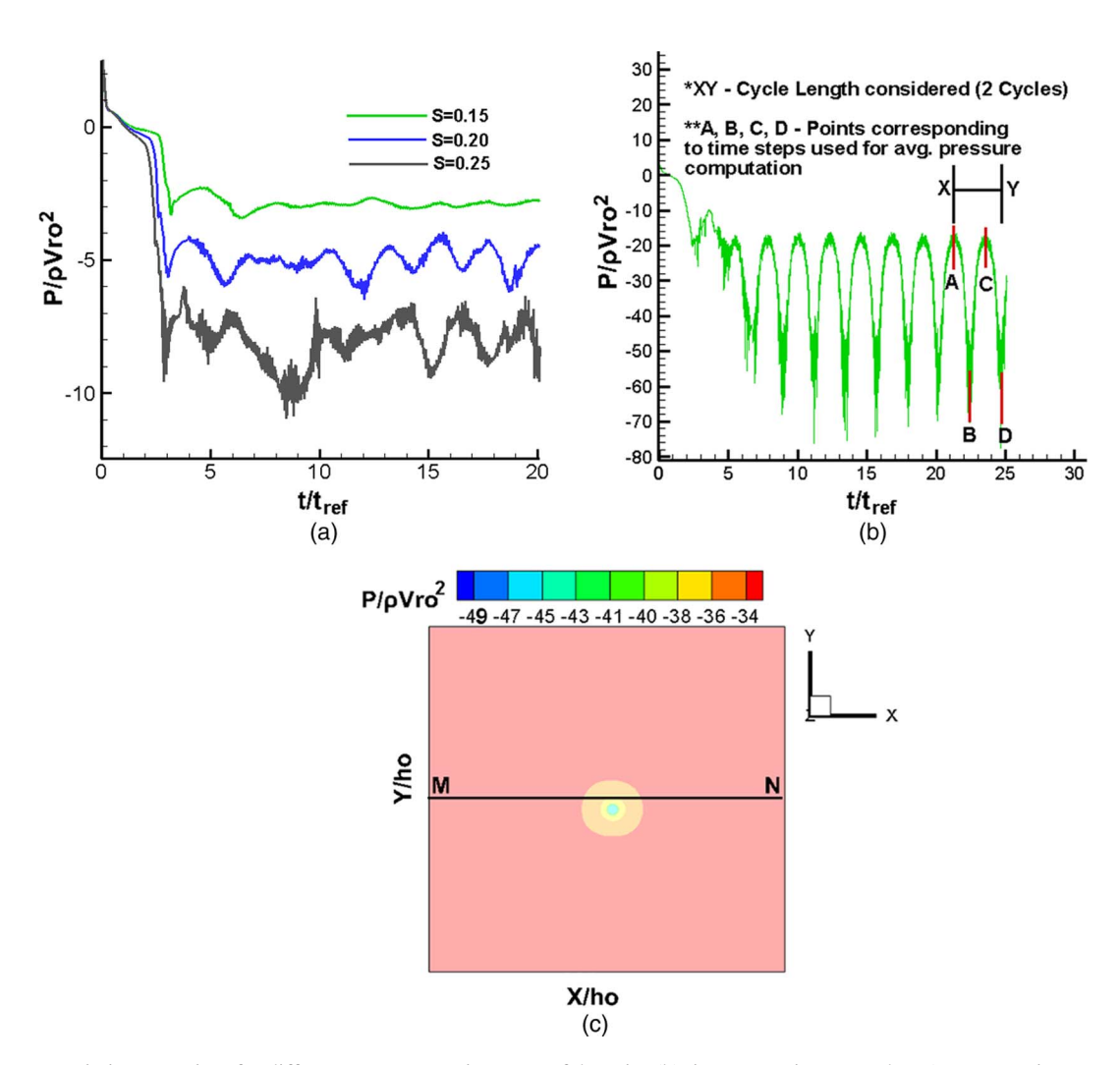


Fig. 5. (a) Pressure variation over time for different S at geometric center of domain; (b) time averaging procedure (representative case of S = 0.60 for illustration); and (c) section line MN used to extract data and obtain pressure profile.

Fig. 5(a), the amplitude of the pressure wave was observed to increase with an increase in S.

The details of time averaging procedure adopted to obtain the mean flow field are as described below:

Once the nature of the variation in the waveform of the flow field variables (pressure and velocity) was understood, as explained in the section "Time-Dependent Flow Phenomena," time averaging was concluded to be necessary to evaluate the mean flow field for further analysis. Thus, the procedure adopted for time-averaging to obtain the mean flow field is explained in detail. As a representative case, the pressure variation at the geometric center of the computational domain for S=0.60 is presented in Fig. 5(b), but the same procedure is adopted for other values of S as well. Because the pressure is varying in a cyclic form, one and a half cycles (represented

by xy) in Fig. 5(b) toward the end of the simulation time was considered for the time-averaging purpose. In that one and a half cycle length, four specific time step values (represented by A, B, C, and D) were picked and were comprised of two peaks and two troughs. Tang et al. (2018) used the mean of 10 values to determine the static mean pressure, whereas the average pressure value in the present study at the geometric center is calculated as the mean of four observations coming from four different time steps. The four values of pressure, consisting of two peaks and two troughs, is assumed to be adequate for capturing the pressure fluctuation over time at a given point, at this instant. To calculate the pressure along line MN in Fig. 5(c), at each point, this procedure is followed to calculate the average pressure.

The complexity of the flow inside the tornado vortex chamber is not only limited to transition in time. However, a spatial transition also forms an essential part that contributes to the added complexity in a tornado chamber flow. These spatial transition phenomena are described in the literature by a term called "vortex wandering" (Refan and Hangan 2016; Gairola 2019) and is explained in the section "Phenomena of Vortex Wandering." Refan and Hangan

(2018) used the technique of azimuthal averaging to minimize the error in the mean pressure field due to vortex wandering; however, no documentation of either vortex wandering or azimuthal averaging existed in Tang et al. (2018). Therefore, in this study, the spatial transition is not presently taken into account.

Phenomena of Vortex Wandering

Vortex wandering can be defined as the spatial shifting of the tornado vortex core in the ground surface plane in a given frame of reference attached to a stationary observer. Also observed is that the wandering of the vortex core is more at lower swirl ratios compared with higher ones, as indicated in Figs. 6 and 7. At a lower *S*, the vortex is in a very unstable state and may be the reason for greater wandering of the vortex core.

To further explore the wandering effect of the vortex in the present CFD model, a reference point was established at the center of the computational domain formed by the intersection of two orthogonal lines, as indicated in Fig. 6. The lowest contour level spot in the figures represents the core of the tornado vortex because

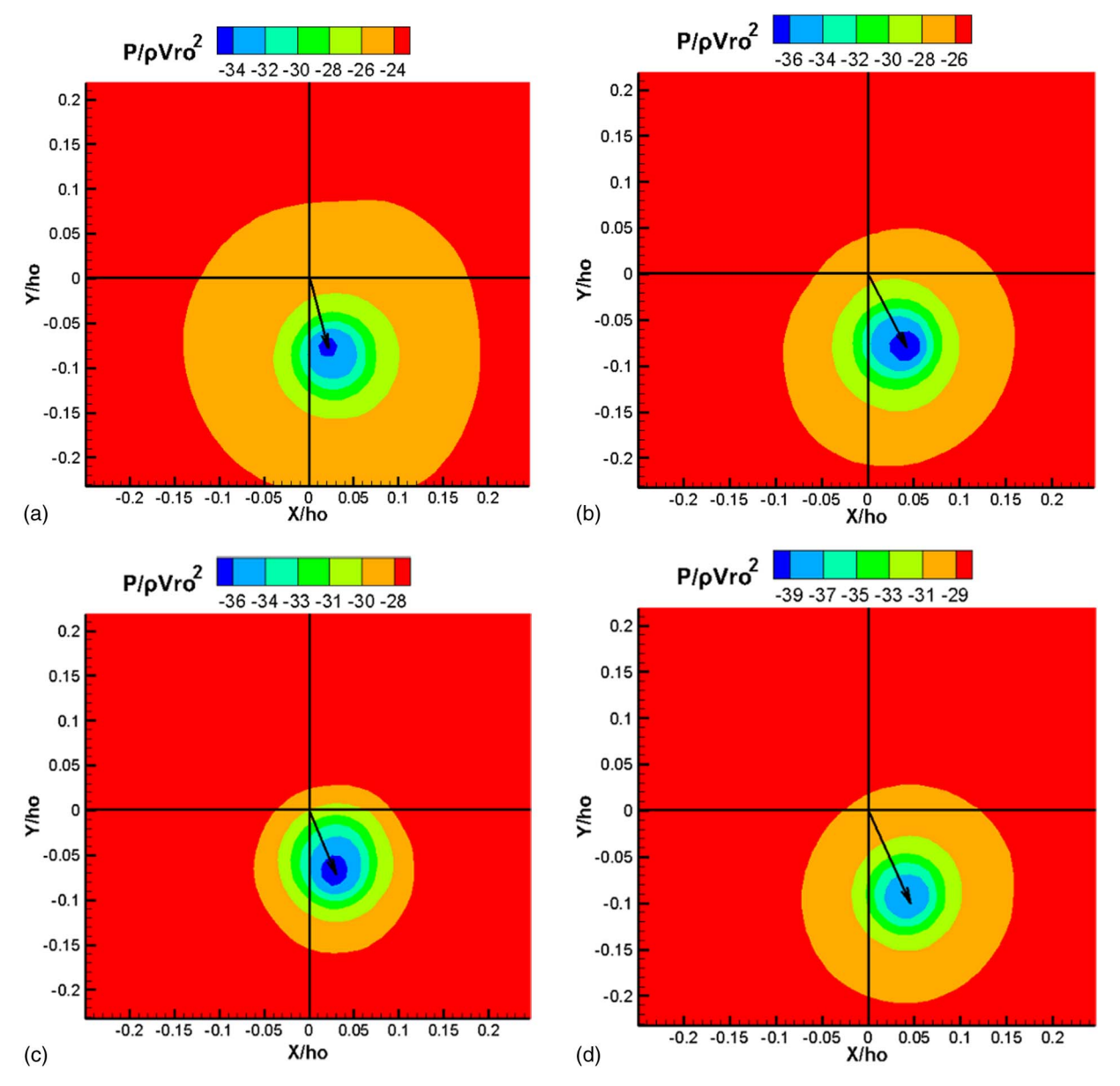


Fig. 6. Transient vortex core with respect to time for S = 0.10 case at t^* : (a) 19.55; (b) 20.62; (c) 22.01; and (d) 23.97.

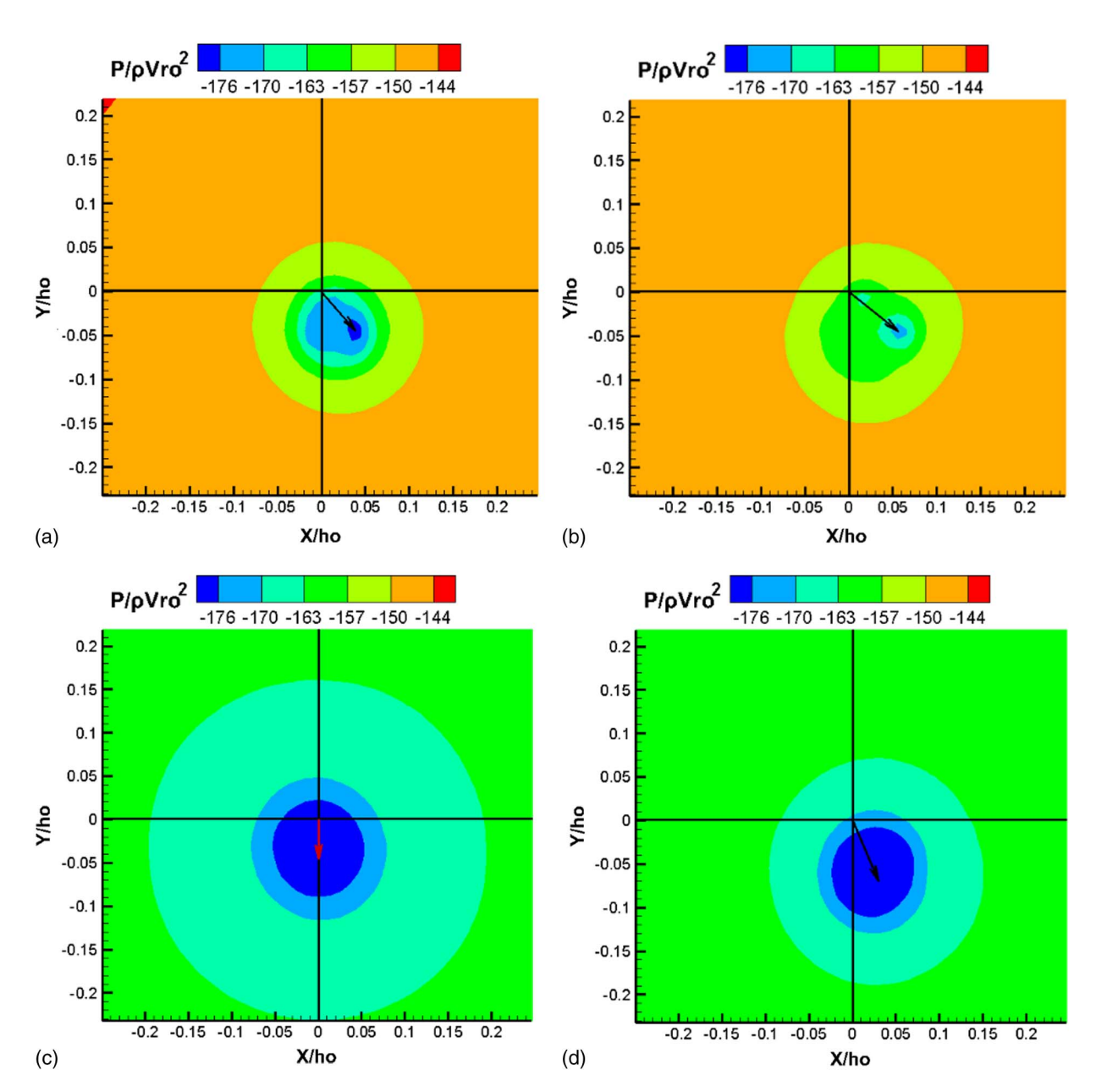


Fig. 7. Transient vortex core with respect to time for S = 0.40 case at t^* : (a) 22.17; (b) 23.36; (c) 24.31; and (d) 24.97.

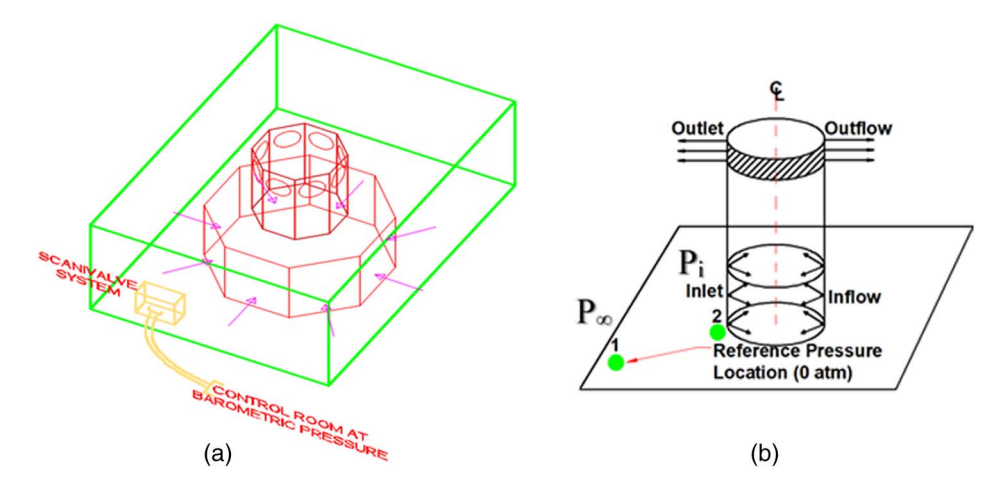


Fig. 8. Reference location for reference pressure consideration: (a) TTU chamber; and (b) CFD chamber.

the sharpest drop in pressure occurs for that spot. An arrow originating from the center of the computational domain with its arrowhead embedded inside the core tracks the centroid of the vortex core (representative of the c.g. of the vortex core). The distance between the tornado vortex core center and the center of the computational domain were determined for different time-steps for S=0.10, and the averaged spatial shift of the tornado core center relative to the center of the computational domain was found to be 0.087 h_o . The standard deviation was 0.015 h_o , and the coefficient of variation was found to be 17.414%.

Similarly, for S = 0.40, the average spatial shift of the tornado core center relative to the center of the computational domain was found to be $0.060 h_o$ with a standard deviation of $0.054 h_o$.

Determination of Reference Pressure

Before the flows at different *S* values including the radial pressure distribution could be analyzed, some reference pressure had to be established relative to which the pressure at different points in the computation domain could be defined because the flow at each different *S* is a unique and independent flow condition. Thus, for a precise and collective representation of the ground pressure

distribution for different S, the pressure at the inlet for different S was determined by taking the normal atmospheric pressure (0 atm gauge pressure) as the reference pressure, and the pressure distribution is obtained relative to this value. In the experimental simulation, Tang et al. (2018) also used the barometric pressure in a static bottle as the reference pressure to obtain pressure measurements relative to a reference value and to avoid errors in pressure measurements from possible fluctuations in the barometric pressure. In the following texts, P_{∞} and P_i represent the pressure values in sections 1 and 2, respectively, as indicated in Fig. 8(b).

At section 1, the assumption $P_{\infty} = V_{\infty} = 0$ can be applied. whereas at inlet point (i) located at section 2, $V_i^2 = V_r^2 + V_t^2$ is applicable. Using Eq. (2) for V_t with $h_o/r_o=1$, an expression of the form $V_i^2 = (1+4S^2)V_r^2$ can be obtained. Applying Bernoulli's theorem between sections 1 and 2 and using the expression of V_i^2 in section 2 yields the expression indicated in Eq. (3). In the nondimensional form, using ρV_{ro}^2 as the normalizing factor, the nondimensional pressure P_i^* is obtained as $P_i^* = -(1+4xS^2)/2$

$$Pi/\rho = \frac{-(1+4xS^2)}{2} \times V_{ro}^2$$
 (3)

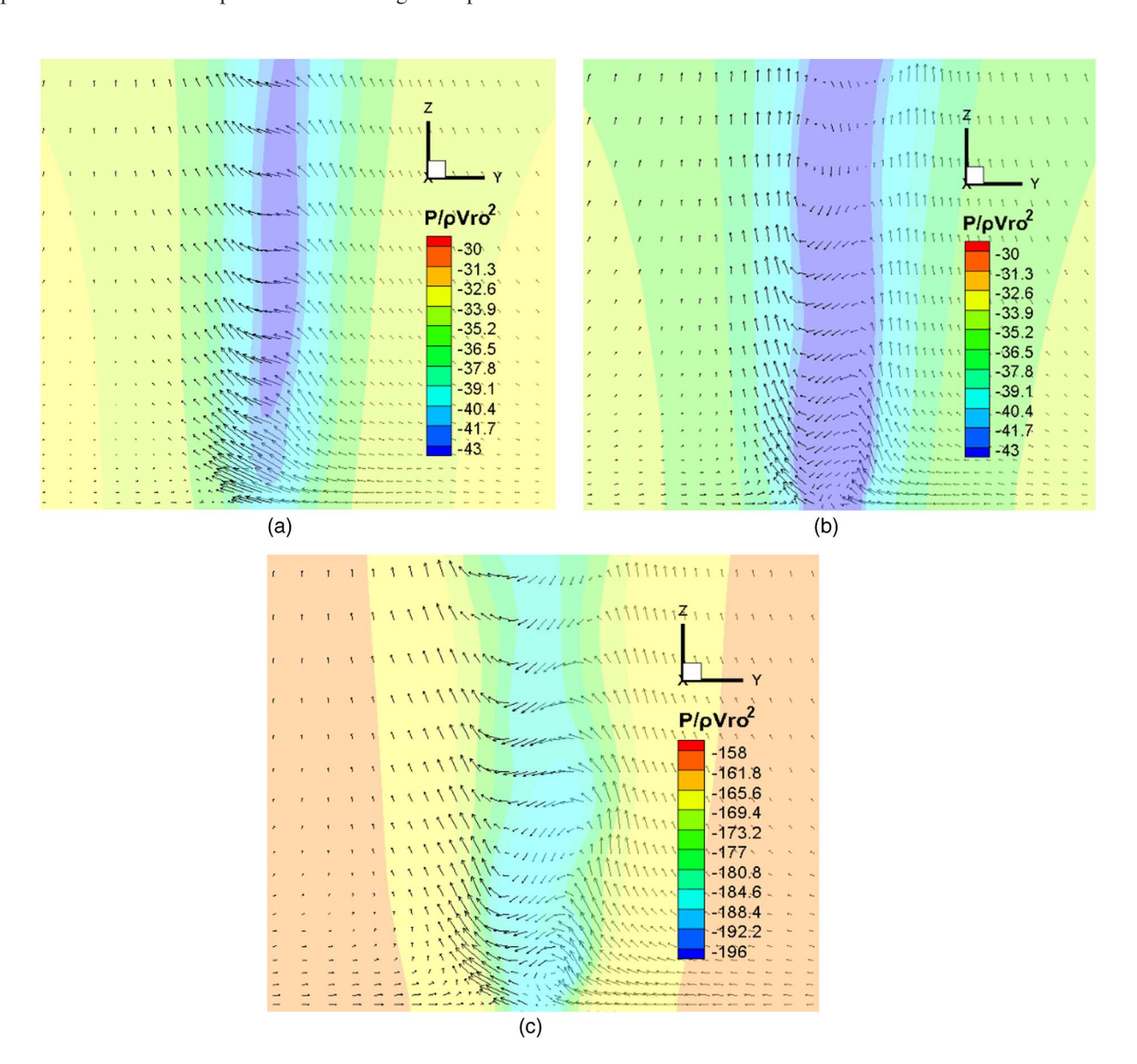


Fig. 9. Velocity vector diagram and pressure contour at vortex core: (a) S = 0.15; (b) S = 0.22; and (c) S = 0.40.

Once the pressure at the inlet is determined using Eq. (3) for a particular value of S, from CFD, the radial distribution of the pressure along the diametric axis of the vortex chamber for that particular value of S can be easily traced. Thus, the radial distribution of pressure for each unique value of S can be represented collectively in a single plot in which the pressure values are mapped relative to a common benchmark pressure value of $P_{\infty}^* = 0$. This approach eliminates the need to use an outer box and vanes, as indicated in Fig. 8(a). The outer box modeling with the vanes is done by Gairola and Bitsuamlak (2019) and Fangping et al. (2016). This approach results in higher computer storage and computing time requirement and reduces the resolution that can be achieved through a simplified CFD model, such as that considered in the current study.

Touchdown S and Effect of Varying S on Radial Ground Pressure Distribution

The computed flow fields for S = 0.15, 0.22, and 0.40 are indicated in Fig. 9. In the current study, as the values of S increased from S = 0.10, touchdown finally occurred at S = 0.22. This S value is in good agreement with the range of S = 0.22-0.36, as reported in Tang et al. (2018). The plots in Fig. 9 illustrate the different stages of tornado vortex development and transition from

a single-celled structure to a double-celled system with increasing *S* values.

In the present study, the radial ground pressure distribution due to the tornado displays a sharp drop in pressure in the core, which complies well with previous studies (Refan and Hangan 2016; Snow et al. 1980). The drop in pressure in the core of the tornado increases first with increasing S and attains a maximum drop, as indicated in Fig. 10(a) for S = 0.60, after which the pressure drop decreases momentarily for S = 0.80. At S = 1.0, the sharp peak in the core, as observed in previous cases (S < 0.80), disappears to take a double valley-shaped structure, as reported in Tang et al. (2018)—roughly symmetrical about the center of the domain. This particular condition of S indicates the existence of a double vortex system on the ground surface, as displayed in Fig. 10(b).

With successive increases in S after the double vortex is observed (S > 1.0), the double vortex is suspected to intensify with increasing S; therefore, the pressure continues to increase with increasing S in the fashion observed for a single-celled vortex with increasing S prior to touchdown. Splitting a single vortex core into two vortices weakens the sharp pressure gradient because now two vortices exist in the flow system that are separated by a distance between them, relieving the pressure gradient and attaining a relatively flatter shape than the earlier cases of S. These observations

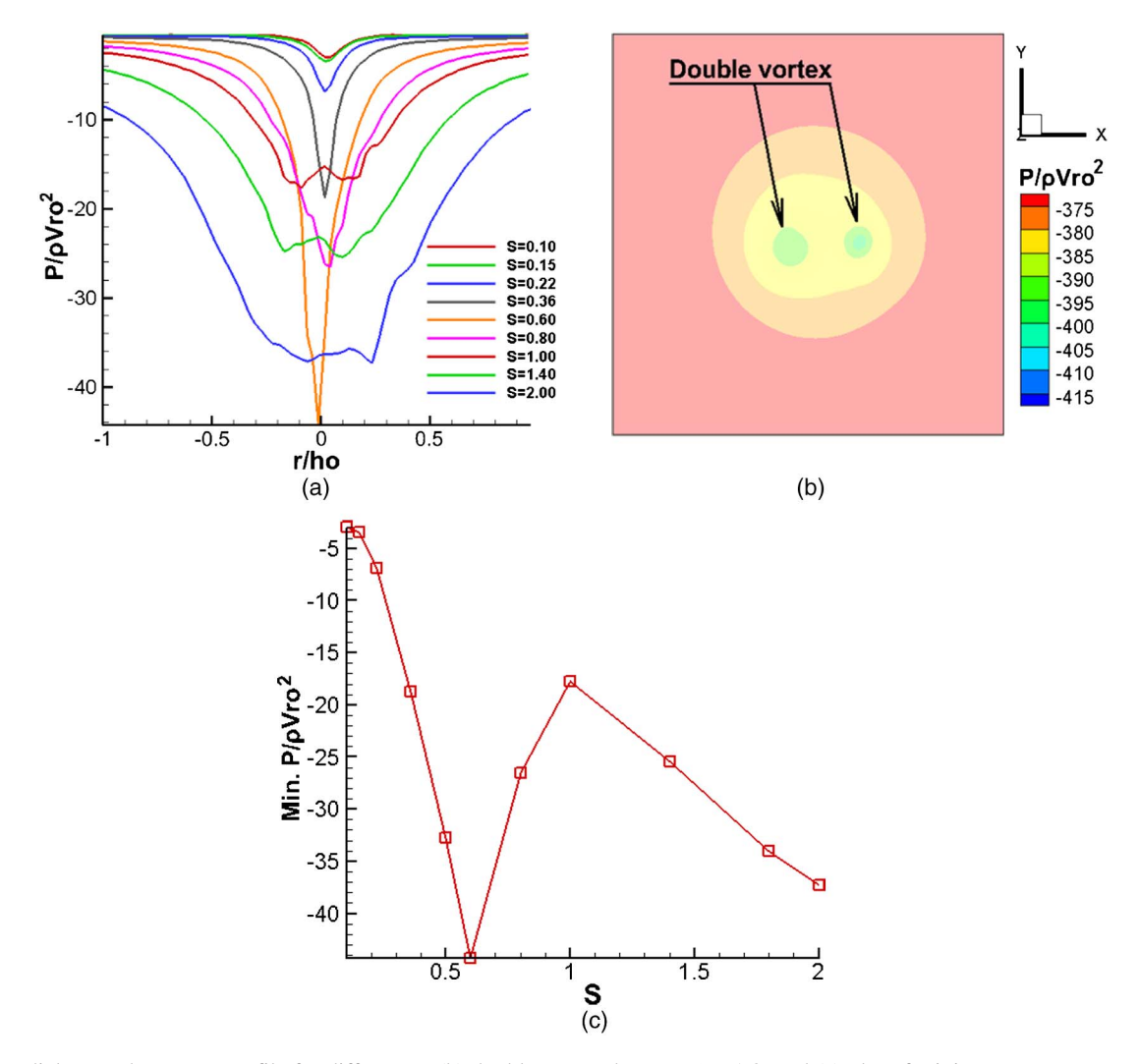


Fig. 10. (a) Radial ground pressure profile for different S; (b) double vortex demo at S = 1.0; and (c) plot of minimum pressure versus swirl ratio.

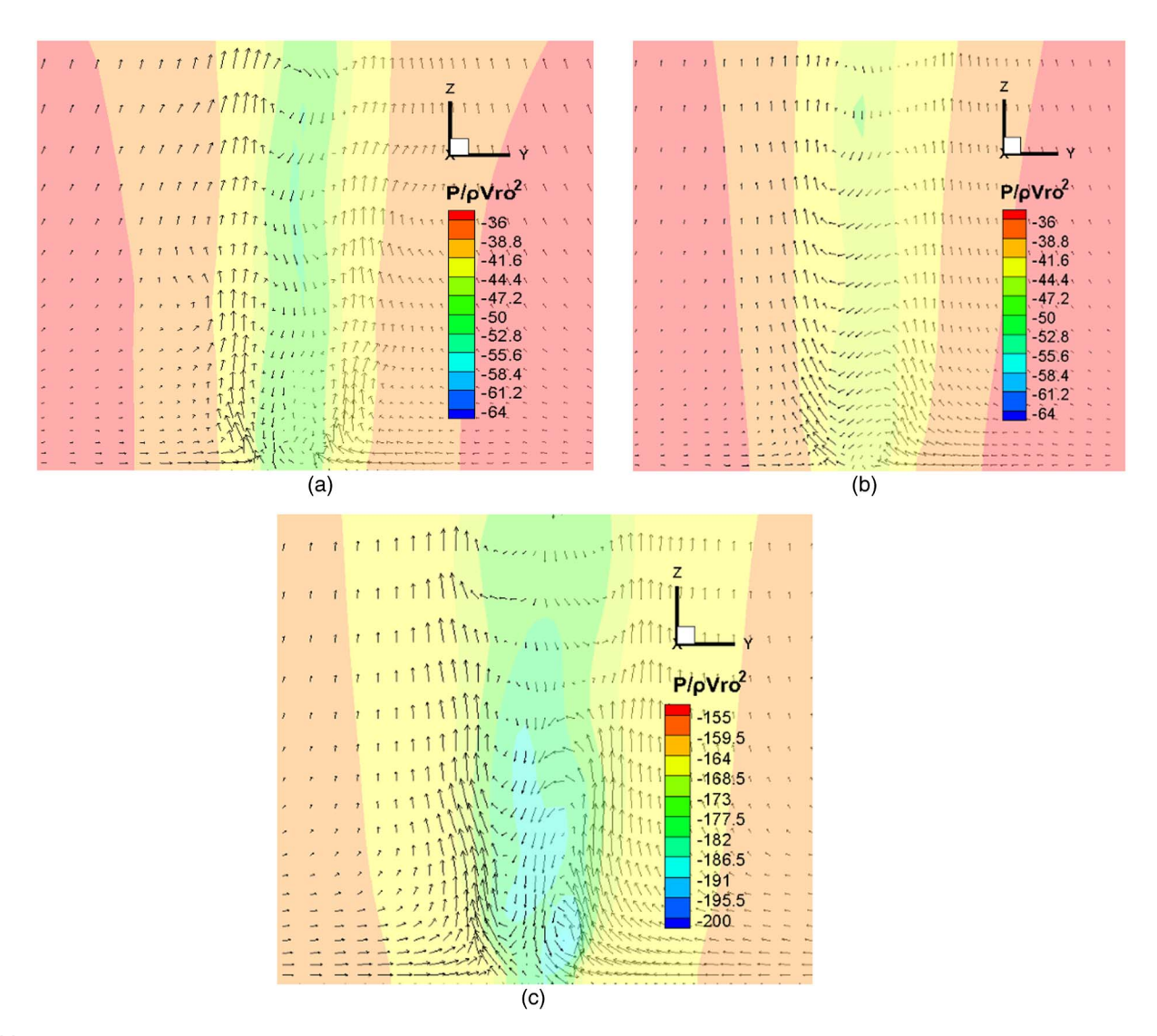


Fig. 11. Tornado touchdown with effective hole size of 0.4 h_o : (a) $Z_o = 0.00001 h_o$, S = 0.15; (b) $Z_o = 0.00004 h_o$, S = 0.22; and (c) $Z_o = 0.00009 h_o$, S = 0.40.

indicate an overall good agreement with Tang et al. (2018) except for differing in one aspect. The increase in the pressure drop with increasing S values and the formation of a double valley-shaped structure that is roughly symmetrical about the domain center in the pressure plot are the key aspects that comply well with the experimental observations of Tang et al. (2018), whereas the greatest drop in pressure is recorded for S = 0.22 in Tang et al. (2018). In the present study, the greatest drop in pressure is reported at S =0.60. Time-dependent flow phenomena and vortex wandering pose significant challenges for precise pressure measurements in both experimental and numerical simulators. For this reason, the discrepancy is suspected to have occurred. The plot of the minimum average pressure against the swirl ratio (S) depicts a valley-shaped curve, as indicated in Fig. 10(c), which generally well follows the trend of the TTU experiment, as reported in Tang et al. (2018), except for minor deviations.

Despite some differences, to be noted is that the CFD model closely follows the trend of TTU experiments. Thus, if certain additional parameters that influence near-surface flows are identified along with further close geometrical idealization of the vortex chamber, then the model indicates its promise to replicate the flow field of the TTU vortex chamber.

Effect of Ground Roughness Variations on Tornado Touchdown

The vortex generated in the TTU chamber is over a flexi-glass surface, as described in Tang et al. (2018). To replicate similar roughness conditions in the CFD model and due to the unavailability of a precise roughness length for glass, a sea surface was chosen as the reference surface because of the similarity in the surface smoothness of the two. Simiu and Scanlan (1978) provide a roughness length range of (0.0003–0.5 cm) for the sea surface; thus, a value of 0.008 cm (0.00004 h_o nondimensional form) is used for the current work.

Given roughness parameters of $Z_o=0.00004\,h_o$ and $C_1=0.0924\,V_{ro}$ (base case), touchdown was found to occur at S=0.22. To study the effect of roughness variation on touchdown, the roughness was decreased with respect to the base case condition, and the touchdown was found to occur at S=0.15 for $Z_o=0.00001\,h_o$ and $C_1=0.0819\,V_{ro}$. Similarly, an increase in roughness with respect to the base case condition resulted in touchdown at S=0.40 for $Z_o=0.00009\,h_o$ and $C_1=0.0999\,V_{ro}$. The pressure contour with velocity vector plots for all three cases is provided in Fig. 11.

These observations illustrate that the critical touchdown swirl ratio increases with increasing roughness parameters and viceversa. These observations are consistent with that of Natarajan and Hangan (2012).

Conclusions

- A method to calculate the inlet pressure with respect to the reference pressure using Bernoulli's theorem is presented for any swirl ratio S. This approach eliminates the need to use an outerbox and vanes and, hence, becomes very efficient with respect to storage and computing time requirements. Furthermore, the domain modeling challenges and complexity are significantly reduced.
- 2. The time-dependent phenomena are observed on account of unsteadiness in flow. Thus, for a particular flow condition (such as with certain *S*), averaging of flow properties over time is required to determine its mean value at a particular point in space. Moreover, the increasing swirl ratio has an enhancing effect on flow unsteadiness as the pressure wave amplitude rises with increasing *S*.
- 3. The core of the tornado vortex was found to be wandering in space and time. On average, the tornado vortex core was found to offset from the geometric center of the computational domain by an average distance of 17.40 cm for S = 0.10 but was found to offset by an average distance of 12.0 cm for S = 0.40. This finding indicates that the wandering effect is severe for low S values.
- 4. The increase in the pressure drop with increasing S values for S < 0.60 and the formation of a double valley-shaped structure roughly symmetrical about the domain center are the key aspects that comply well with TTU observations, whereas the S value for the occurrence of a maximum pressure drop indicates a contrast between them. Therefore, the conclusion reached is that general agreement exists in the pressure profile obtained through the CFD model, which follows the trend of the TTU experiment well but with some differences in minutiae.
- 5. Increasing the ground roughness increases the critical touchdown swirl ratio and vice-versa. Increasing the ground roughness has a similar effect to converting the flow into a lower swirl flow configuration. Moreover, the vortex breakdown and touchdown were observed to initiate and occur under the influence of increasing *S*. A combination of the two arguments confers that the critical touchdown *S* should increase with increasing roughness, and the reverse is also true.

A comparable and working CFD model similar to the TTU vortex chamber has been developed. Further work on the interaction of the tornado vortex with the building is underway to determine the pressure and force coefficients on the building, the detailed account of which will be reported in future studies.

Data Availability Statement

Some or all of the data, models, or code generated or used during the study are available from the corresponding author by request: 1. All data.

2. Details of computational model.

.

Acknowledgments

The authors acknowledge the support received from the National Science Foundation under award number CMMI-1762999.

References

- Cengel, Y. A., and J. M. Cimbala. 2014. Fluid mechanics: Fundamentals and applications. 3rd ed. New York: McGraw Hill.
- Fangping, Y., Y. Guirong, H. Ryan, K. M. Isaac, and F. Ruoqiang. 2016. "Effects of chamber shape on simulation of tornado-like flow in a laboratory." In *Wind engineering for natural hazards-modeling, simulation, and mitigation of windstorm impact on critical infrastructure*, edited by A. Mousaad Aly and E. Dragomirescu. Reston, VA: ASCE.
- Gairola, A. 2017. Generic numerical tornado model for common interpretation of existing experimental simulators. Ph.D. thesis, Dept. Civil and Environmental Engineering, Univ. of Western Ontario.
- Gairola, A., and G. Bitsuamlak. 2019. "Numerical tornado modeling for common interpretation of experimental simulators." *J. Wind Eng. Ind. Aerodyn.* 186 (Mar): 32–48. https://doi.org/10.1016/j.jweia.2018.12.013.
- Haan, F. L., P. P. Sarkar, and W. A. Gallus. 2008. "Design, construction and performance of a large tornado simulator for wind engineering applications." *Eng. Struct.* 30 (4): 1146–1159. https://doi.org/10.1016/j .engstruct.2007.07.010.
- Hangan, H. 2014. "The wind engineering energy and environment (WindEEE) Dome at Western University, Canada." Wind Eng. JAWE 39 (4): 350–351. https://doi.org/10.5359/jawe.39.350.
- Hirt, C. W., and J. L. Cook. 1972. "Calculating three-dimensional flows around structures and over rough terrain." *J. Comput. Phys.* 10 (2): 324–340. https://doi.org/10.1016/0021-9991(72)90070-8.
- Ishihara, T., S. Oh, and Y. Tokuyama. 2011. "Numerical study on flow fields of tornado-like vortices using the LES turbulence model." J. Wind Eng. Ind. Aerodyn. 99 (4): 239–248. https://doi.org/10.1016/j.jweia .2011.01.014.
- Kashefizadeh, M. H., S. Verma, and R. P. Selvam. 2019. "Computer modelling of close-to-ground tornado wind-fields for different tornado widths." J. Wind Eng. Ind. Aerodyn. 191 (Aug): 32–40. https://doi.org /10.1016/j.jweia.2019.05.008.
- Kikitsu, H., Y. Okuda, H. Kawai, and J. Kanda. 2012. "Experimental study on characteristics of tornado-induced wind force on a low-rise building." In *Proc.*, 22nd National Symp. on Wind Engineering, 209–214. https://doi.org/10.14887/kazekosymp.22.0.209.0.
- Leonard, B. P. 1979. "A stable and accurate convective modelling procedure based on quadratic upstream interpolation." *Comput. Methods Appl. Mech. Eng.* 19 (1): 59–98. https://doi.org/10.1016/0045-7825 (79)90034-3.
- Liu, Z., and T. Ishihara. 2015. "A study of tornado induced mean aerodynamic forces on a gable-roofed building by the large eddy simulations." J. Wind Eng. Ind. Aerodyn. 146 (Nov): 39–50. https://doi.org/10.1016/j.jweia.2015.08.002.
- Matsui, M., and Y. Tamura. 2009. "Influence of swirl ratio and incident flow conditions on generation of tornado-like vortex." In *Proc.*, *EACWE 5*. Florence, Italy: Firenze University Press. https://doi.org/10 .1400/116522.
- Natarajan, D., and H. Hangan. 2012. "Large eddy simulations of translation and surface roughness effects on tornado-like vortices." J. Wind Eng. Ind. Aerodyn. 104–106 (May): 577–584. https://doi.org/10.1016/j.jweia .2012.05.004.
- Refan, M., and H. Hangan. 2016. "Characterization of tornado-like flow fields in a new model scale wind testing chamber." J. Wind Eng. Ind. Aerodyn. 151 (Apr): 107–121. https://doi.org/10.1016/j.jweia.2016.02.002.
- Refan, M., and H. Hangan. 2018. "Near surface experimental exploration of tornado vortices." J. Wind Eng. Ind. Aerodyn. 175 (Apr): 120–135. https://doi.org/10.1016/j.jweia.2018.01.042.
- Selvam, R. P. 1997. "Finite element modelling of flow around a circular cylinder using LES." J. Wind Eng. Ind. Aerodyn. 67–68 (Apr): 129– 139. https://doi.org/10.1016/S0167-6105(97)00068-8.
- Selvam, R. P., and P. C. Millett. 2003. "Computer modeling of tornado forces on a cubic building using large eddy simulation." J. Arkansas Acad. Sci. 57 (1): 140–146.
- Selvam, R. P., and S. Verma. 2019. "Comparison of CFD model touchdown flow field with TTU experiment." In *Proc.*, 15th Int. Conf. on Wind Engineering (ICWE15). Beijing, China: Tongji Univ.

- Simiu, E., and R. Scanlan. 1978. Wind effects on structures. New York: Wiley.
- Snow, J. T., C. R. Church, and B. J. Barnhart. 1980. "An investigation of the surface pressure fields beneath simulated tornado cyclones." J. Atmos. Sci. 37 (5): 1013–1026. https://doi.org/10.1175/1520-0469 (1980)037<1013:AIOTSP>2.0.CO;2.
- Tang, Z., C. Feng, L. Wu, D. Zuo, and L. Wu. 2018. "Characteristics of tornado-like vortices simulated in a large scale ward type simulator." *Boundary Layer Meteorol.* 166 (2): 327–350. https://doi.org/10.1007/s10546-017-0305-7.
- Versteeg, H. K., and W. Malalasekera. 2007. An introduction to computational fluid dynamics the finite volume method. London: Pearson Education.